Low-energy electronic excitation in atomic collision cascades: A nonlinear transport model

A. Duvenbeck and A. Wucher*
Department of Physics, University of Duisburg-Essen, D-47048 Duisburg, Germany
(Received 30 May 2005; published 7 October 2005)

A computer simulation model is presented which allows one to incorporate low-energy electronic excitation into the molecular dynamics computer simulation of atomic collision cascades in metals. The model treats the electronic energy losses experienced by all moving atoms as a source term for electronic excitation energy, which is assumed to spread around the original point of excitation with a diffusivity D. In order to acknowledge (i) the large temperature gradients and (ii) the local lattice disorder within the cascade volume, the electronic heat diffusivity is allowed to vary as a function of space and time, thus leading to a strongly *nonlinear* diffusion of electronic excitation energy. The corresponding diffusion equation is developed and numerically solved for an exemplary collision cascade initiated by the impact of a 5 keV silver atom onto an Ag(111) surface. It is shown that electron surface temperatures of several thousand kelvin can be reached at times after the impact at which most emission of surface particles occurs. This excitation may therefore influence the ionization or excitation of such sputtered species.

DOI: 10.1103/PhysRevB.72.165408 PACS number(s): 79.20.Ap, 71.10.Ca, 71.10.Li

I. INTRODUCTION

When a solid is bombarded with keV-ions, particles are removed ("sputtered") from the surface due to the evolution of an atomic collision cascade. It is well known that the atomic motion induces electronic excitation processes which manifest, for instance, in the observation of kinetic electron emission[1] or the occurence of excited or ionized states among the flux of sputtered particles.[2]

Due to the fact that an *ab initio* treatment of a system large enough to envelope a keV-impact-induced collision cascade is still prohibitively complex, simplified models[3–10] have been proposed for the incorporation of electronic excitation processes into standard classical molecular dynamics (MD) computer simulations.[11] Most of these models assume *electron promotion*[12] in close binary atomic collisions to be the fundamental excitation mechanism.

We have developed an alternative concept[13] for ion-bombarded metals wherein the transfer of kinetic into electronic excitation energy is described in the frame of a quasi-free electron gas model. It is assumed that the friction-like electronic energy loss experienced by all moving atoms leads to a space- and time-dependent electronic excitation that spreads around the original point of generation with a diffusivity D. The resulting excitation energy density $E(\vec{r},t)$ is parametrized in terms of a space- and time-dependent electron temperature $T_e(\vec{r},t)$. Although the underlying assumption of quasi-instantaneous energy equipartition among the electron system is not generally justified, we argue that the original energy spectrum generated by electronic friction is dominated by low-energy excitations and therefore closely resembles a Fermi distribution at all times.[14]

In first computer simulations,[13] this model has been applied to calculate electronic excitations during sputtering of an Ag(111) monocrystalline surface under bombardment with an atomic silver projectile. Self-sputtering conditions have been chosen in order to avoid any chemical complexity that might otherwise influence the collision or excitation dynamics. The corresponding many-body interaction potential function[15] has been used in a number of previous studies[16,17] and was found to produce results in good correspondence with experimental data.

The electronic excitation calculations performed in Ref. 13 have demonstrated that, for the model system employed here, electron temperatures T_e of several thousands of kelvin may be reached, which are large enough to influence the electronic states of emitted particles. However, the numerical approach employed in our former study limited the model to *constant* or at most *time-dependent* diffusivity D.

It is well known that the evolution of an atomic collision cascade leads to a time- and position-dependent reduction of crystallographic order within the solid. As a consequence, the electron mean-free path λ and hence the diffusivity D will exhibit strong local and temporal variations.

In the present work, we therefore extend our model towards a full three-dimensional treatment based on a finite-differences (FD) approach that allows for a spatial variation of D. The latter, in turn, is correlated with both the lattice and the electron temperature at each point in space and time. In addition, we incorporate a local order parameter that is calculated from the time-dependent atom positions delivered by the MD calculation. This parameter is then used to interpolate the local diffusivity D between values appropriate for an ideal crystal and a fully amorphized solid, respectively. Results show that the atomic disorder plays a key role in trapping the electronic excitation in the cascade volume. The resulting time dependence of the electron temperature T_e is calculated as a function of position around the impact point.

II. DESCRIPTION OF THE MODEL

A. Molecular dynamics

We use a standard molecular dynamics code described in detail earlier[16] to follow the temporal and spatial evolution of the atomic collision cascade. In short, the classical Newtonian equations of motion are integrated numerically for all

target atoms and the projectile. In our case we use an fcc model crystallite consisting of about 4500 atoms distributed over 18 atomic layers with a nonreconstructed (111)-oriented surface. The interaction among all atoms is described by a MD/MC-CEM many-body potential,[15] which has been fitted to the properties of silver.

B. Electronic excitation mechanism and transport

The electronic system in our model is represented by a quasi-free electron gas with Fermi energy E_F and an electron mean-free path λ. The electronic energy loss per unit track length experienced by a particle with kinetic energy E_k is treated within the Lindhard model[18] of electronic friction as

$$\frac{dE_k}{dt} = -Kv^2 = -AE_k, \tag{1}$$

where A is a constant evaluated as 2.9×10^{12} s^{-1} for the specific case of an Ag atom moving in silver. The amount dE of excitation energy fed into the electron gas per time interval dt at the position $\vec{r}$ is then

$$\frac{dE(\vec{r},t)}{dt} = A\sum_i E_k^i(t)\cdot\delta(\vec{r}_i-\vec{r}) = AE_k(\vec{r},t), \tag{2}$$

where $E_k^i(t)$ denotes the kinetic energy of the ith particle moving at $\vec{r}_i$ and time t. These quantities are taken from the MD simulation. The temporal and spatial spread of the excitation energy $E(\vec{r},t)$ is modeled by a numerical solution of the three-dimensional diffusion equation. The corresponding diffusion coefficient or diffusivity D constitutes the essential physical input parameter of the model. In the particular case of a *constant* diffusion coefficient, the equation reads

$$\frac{\partial E(\vec{r},t)}{\partial t} - D\nabla^2E(\vec{r},t) = \left(\frac{dE(\vec{r},t)}{dt}\right)_s, \tag{3}$$

which can be solved in a straightforward manner using a Green's function method.[13,19]

In the following, we will expand the versatility of the approach by allowing D to depend on the lattice temperature T_l, the calculated electron temperature T_e itself, and an additional lattice order parameter $\Lambda(\vec{r},t)$. The exact functional form of D will be discussed in the following subsection. The corresponding diffusion equation

$$\frac{\partial E(\vec{r},t)}{\partial t} - \vec{\nabla}\cdot[D(T_l(\vec{r},t),T_e(\vec{r},t),\Lambda(\vec{r},t))\vec{\nabla}E(\vec{r},t)] = \left(\frac{dE(\vec{r},t)}{dt}\right)_s. \tag{4}$$

is no longer linear in $E(\vec{r},t)$, thereby complicating the numerical treatment. In particular, it is no longer possible to solve Eq. (4) by means of a simple Green's function approach. Instead, we revert to a finite-differences treatment described in detail below.

C. Diffusion coefficient

In principle, the diffusivity D of electronic excitation energy can be evaluated as

$$D = \frac{1}{3}\lambda v_F, \tag{5}$$

where λ denotes the mean-free path of the electrons and v_F is the Fermi velocity. Under nonequilibrium conditions characterized by an electron temperature T_e and a lattice temperature T_l—both varying in space and time—the mean-free path in a perfectly crystalline solid is given by[20]

$$\lambda = \frac{v_F}{aT_e^2 + bT_l}. \tag{6}$$

The first term in the denominator of Eq. (6) arises from electron-electron scattering, while the second term originates from electron-phonon scattering. For silver, the constants are estimated as $a\approx1.2\times10^7$ K^{-2} s^{-1} and $b\approx1.2\times10^{11}$ K^{-1} s^{-1}.[20] The electron temperature T_e in Eq. (6) is calculated from $E(\vec{r},t)$ using the electronic specific heat,[21] as

$$c_e = \frac{\pi^2}{2}\cdot n_e\cdot k_B\frac{T_e}{T_F} =: C\cdot T_e \tag{7}$$

(k_B: Boltzmann constant, n_e: electron density, T_F: Fermi temperature) of the conduction electrons in the solid as

$$T_e = \sqrt{\frac{2}{C}E + T_{e,0}^2}. \tag{8}$$

In Eq. (8) $T_{e,0}$ denotes the initial electron temperature prior to the projectile impact.

At this point, we would like to stress that the procedure outlined above is not meant to imply quasi-instantaneous thermalization of the electronic excitation energy. As correctly pointed out, for instance, in Ref. 22, the mean-free path for electron-electron scattering as determined by Eq. (6) is generally larger than the dimension of the cascade, precluding the establishment of local thermal equilibrium within the electronic subsystem. On the other hand, recent *ab initio* simulations based on time-dependent density functional theory[14] reveal that the excitation spectrum produced by a moving atom traversing a metallic solid clearly exhibits an exponential tail. In that respect, it appears that even at low kinetic energies of the order of several eV the excitation mechanism itself produces a spectrum closely resembling a Fermi distribution, which can be parametrized by a somewhat artificial electron temperature T_e.

The lattice temperature T_l entering Eq. (6) is calculated as

$$T_l(\vec{r},t) = \frac{2E_k^{tot}(\vec{r},t)}{3Nk_B}, \tag{9}$$

where E_k^{tot} denotes the sum of the relative kinetic energy of all N particles localized within a sphere of radius r_c centered at $\vec{r}$ at time t. The center-of-mass velocity is subtracted in order to exclude a possible influence of directed collective motion.

We are aware that the definition of a lattice temperature is critical because the particle dynamics within the cascade may exhibit a strongly nonequilibrium character. Furthermore, in the simulation we have to make a tradeoff between sufficient particle statistics on the one hand, which demands for large

sphere radii r_c, and on the other hand, a reasonable spatial resolution of the temperature profile requiring small values of r_c. Thus, the calculated values for T_l should be interpreted carefully and should only be regarded as a physical parameter describing the kinetic energy density in the cascade volume rather than a realistic temperature.

Now, substituting Eq. (6) into Eq. (5) yields the expression

$$D_0(\vec{r},t) = \frac{1}{3}\frac{v_F^2}{aT_e^2(\vec{r},t) + bT_l(\vec{r},t)}, \tag{10}$$

where the index zero is meant to underline that disorder effects have not yet been taken into account. At room temperature ($T_e = T_l = 300$ K) the mean-free path resulting from Eq. (6) is of the order of 40 nm. This value is determined exclusively by electron-phonon scattering and yields $D^{cryst} \approx 180\ \mathrm{cm}^2/\mathrm{s}$. We remark that, for that particular case, the mean-free path exceeds the dimension of our model crystal by about one order of magnitude, calling the diffusive approach into question. On the nanometer scale targeted here, the transport of excitation energy within a quiescent ideal crystal should therefore be described more realistically in terms of ballistic motion rather than by a diffusion mechanism. However, as shown below, the rapid lattice heating, combined with the effect of local disorder, leads to a drastic reduction of λ and D within the first few femtoseconds of a collision cascade, thereby justifying the diffusive treatment at later times.

So far, we have considered the case of a *crystalline* solid under nonequilibrium conditions. A detailed analysis[13] of the time-dependent radial distribution function reveals a rapid destruction of the crystalline order on subpicosecond time scales after the primary particle impact. More specifically, the evolution of the atomic collision cascade induces a rapid loss of long range order, leading to a complete amorphization of the model system within a time interval of approximately 300 fs. In this limit, the concept of electron-phonon scattering must be replaced by quasi-elastic scattering on individual atoms with a mean-free path λ comparable to the mean interatomic distance. The excited electrons will therefore undergo a chaotic motion that can be described rather well by a diffusive approach with a diffusion coefficient of the order of $D^{am} \approx 0.5\ \mathrm{cm}^2/\mathrm{s}$.[22]

In our previous work,[13] the influence of crystalline order has been described only *qualitatively* without spatial resolution by assuming the diffusivity to decrease linearly between D^{cryst} and D^{am} within a time interval of several 100 fs after the projectile impact. While this temporal variation could be easily incorporated into the numerical Green's function method employed to solve the diffusion equation, it allowed no spatial variation of D. The latter, on the other hand, appears to be important due to the strongly local character of the collision cascade dynamics.

In the following, we present an approach to incorporate both the temporal and spatial dynamics of lattice disorder as well as its coupling to the diffusivity D. For that purpose, a scalar, local lattice order parameter is defined at $\vec{r}=(x_1=x, x_2=y, x_3=z)$ by[23]

$$\Lambda(\vec{r},t) = \frac{1}{3N}\left|\sum_i \sum_{j=1}^{3} \cos\left(\frac{2\pi}{a_j} x_j^i(t)\right)\right|, \tag{11}$$

where the outer sum loops over all N particles within a sphere of radius r_c around $\vec{r}$. The parameters a_j denote the nearest neighbor distances in the x_j-directions of the coordinate system. Thus, the case of a completely ordered fcc crystal yields $\Lambda = 1$ because each particle is positioned on a lattice site and therefore each cosine in Eq. (11) is equal to 1. In the case of a completely amorphized crystal, on the other hand, the values of λ fluctuate statistically around zero with an amplitude of the order of $\delta = N^{-1/2}$, provided the cutoff-radius r_c is not too small. In our treatment, we chose a value of $r_c = 8$ Å (corresponding to $\delta \approx 0.05$), which is large enough to include the seventh-nearest-neighbor shell in a silver crystal.

It should be pointed out at this point, that the order parameter considered here is based on rather simple periodicity arguments. More sophisticated definitions of scalar order parameters which, for example, take into account bond-orientation statistics[24,25] can be found in the literature. However, they are significantly more time consuming to calculate. Moreover, Morris and Song[26] have proposed a scalar measure of translational order that is very similar to Eq. (11), but additionally features a time- and neighbor-averaging procedure in order to cancel out artifacts caused by fast atomic lattice vibrations. This averaging procedure, however, would conceal the fast, collision-induced lattice dynamics that are explicitly considered here and therefore would be detrimental to the goal of the present work.

The next step in our model description regards the influence of local disorder on the effective diffusivity D. In principle, it is not trivial to rigorously derive a straightforward relation between Λ and D, which is based on simple arguments. As a zero-order approach, we apply a linear interpolation between the two limiting cases of (i) a completely ordered crystal ($\Lambda = 1$) and (ii) an amorphous ensemble of particles ($\Lambda \approx 0.05$) with

$$D(\Lambda = 1) = D_0 \text{ and } D(\Lambda = 0.05) = D^{am}, \tag{12}$$

leading to

$$D(\vec{r},t) = \frac{D_0(\vec{r},t) - D^{am}}{0.95} \cdot \Lambda(\vec{r},t) + \frac{D^{am} - 0.05 D_0(\vec{r},t)}{0.95}. \tag{13}$$

In combination with Eq. (10), this relation describes the influence of local heating, electronic excitation, and lattice disorder on the excitation energy diffusivity D. Note that the dependence on $\vec{r}$ is implicit via local variations of the electron temperature T_e, lattice temperature T_l, and order parameter Λ.

D. Numerical implementation

The model crystallite of dimension $42 \times 42 \times 42$ Å^3 is discretized into 2744 small cubic volume elements with grid spacing $\Delta = 3$ Å in each direction. The function $E(\vec{r},t)$ is then represented by its values at the discrete set of cell centers

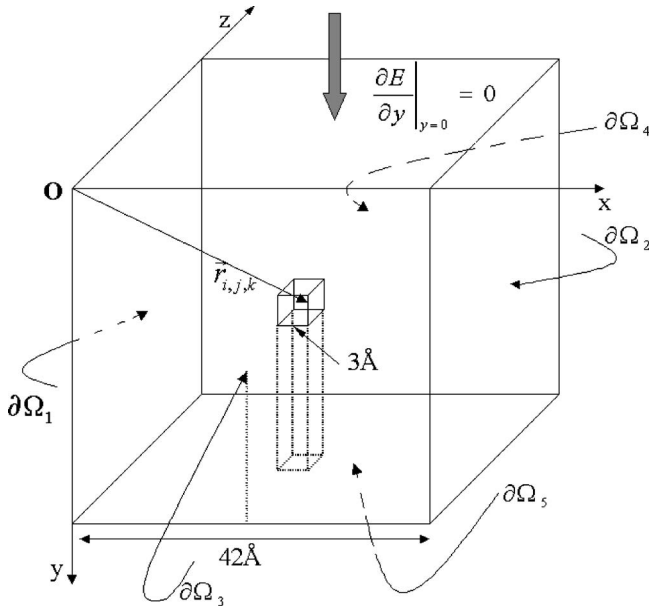

FIG. 1. Schematic drawing showing the boundaries and dimensions, as well as one representative discretization cell.

$\vec{r}_{i,j,k}=i\Delta\cdot\vec{e}_x+j\Delta\cdot\vec{e}_y+k\Delta\cdot\vec{e}_z$ with $(i,j,k)\in\{1,\ldots,14\}^3$ and $\vec{e}_x$, $\vec{e}_y$, and $\vec{e}_z$ denoting the unit vectors in x-, y-, and z-directions, respectively (see Fig. 1).

Let $E^{n=0}_{i,j,k}$ denote the initial excitation energy distribution at time t_0 at $\vec{r}_{i,j,k}$. The resulting distribution $E_{i,j,k}$ at time $t_{n+1}=t_0+(n+1)\Delta t$ is then numerically evaluated as[27]

$$\begin{aligned}E^{n+1}_{i,j,k} = {} & \Delta t\cdot\left(\frac{dE}{dt}\right)_s\Bigg|^n_{i,j,k}+\frac{\Delta t}{\Delta r^2}\{D^n_{i+1/2,j,k}\cdot(E^n_{i+1,j,k}-E^n_{i,j,k})\\ & -D^n_{i-1/2,j,k}\cdot(E^n_{i,j,k}-E^n_{i-1,j,k})+D^n_{i,j+1/2,k}\cdot(E^n_{i,j+1,k}\\ & -E^n_{i,j,k})-D^n_{i,j-1/2,k}\cdot(E^n_{i,j,k}-E^n_{i,j-1,k})\\ & +D^n_{i,j,k+1/2}\cdot(E^n_{i,j,k+1}-E^n_{i,j,k})-D^n_{i,j,k-1/2}(E^n_{i,j,k}-E^n_{i,j,k-1})\}\end{aligned}$$

with

$$\begin{aligned}D^n_{i+1/2,j,k} = {} & \frac{1}{2}\cdot\{D(T^n_{l;i+1,j,k},T^n_{e;i+1,j,k},\Lambda^n_{i+1,j,k})\\ & +D(T^n_{l;i,j,k},T^n_{e;i,j,k},\Lambda^n_{i,j,k})\}.\end{aligned}$$

The boundary conditions for the solution of Eq. (4) are critical. At the surface ($j=1$), a *Neumann* condition $\vec{\nabla}E\cdot\vec{n}=0$ is enforced in the outward direction to prohibit outward diffusion of excitation energy into the vacuum. This is implemented by defining a virtual cell layer at $j=0$ with $E_{i,0,k}:=E_{i,1,k}$.

For the other boundaries of the crystal, the underlying physics require *open* boundary conditions. In order to realize that, we introduce a set of virtual cell layers, which in the following will be refered to as $\partial\Omega_m$ with $m\in\{1,\ldots,5\}$ denoting the left, right, front, back, and bottom virtual cell layers, respectively, with corresponding surface normal vectors $\vec{n}_m$. Each of these virtual layers of cells is directly attached outside the corresponding crystal boundary plane. We then calculate the excitation energy

$$\Delta E^{out,n}=\frac{1}{\Delta r}D_{out}\vec{\nabla}E\cdot\vec{n}_m\Delta t \tag{14}$$

flowing out of each boundary cell during the time interval Δt at time t under the assumption of a *constant* diffusion coefficient D_{out} outside the crystal. These values are stored in a large data matrix and are taken as electronic energy point sources ΔE^s localized at the particular virtual cell in the corresponding virtual cell layer. Since the outward diffusivity is constant, the time evolution of E within these virtual cells is followed using the Green's function formalism. To illustrate this procedure, let $I_m:=\{(i,j,k)\,|\,\vec{r}_{i,j,k}\in\partial\Omega_m\}$ denote the set of indices representing the virtual cells of the mth virtual layer. Formally, the values of E within these virtual cells at time t_n are calculated as[13]

$$\begin{aligned}E(\vec{r}_{i,j,k}\in\partial\Omega_m,t_n) = {} & \sum_{\alpha=0}^{n-1}\sum_{\kappa,\mu,\nu\in I_m}\Delta E^{s,\alpha}_{\kappa,\mu,\nu}\\ & \times\frac{1}{[4\pi D_{out}(t_n-t_\alpha)]^{3/2}}\exp\left(\frac{-|\vec{r}_{\kappa,\mu,\nu}-\vec{r}_{i,j,k}|^2}{4D_{out}(t_n-t_\alpha)}\right)\end{aligned} \tag{15}$$

and are taken as the new boundary conditions for the next finite-differences time step.

As an example to demonstrate the implementation of Eqs. (14) and (15), consider the left crystal boundary plane characterized by a fixed cell index $i=1$. According to Eq. (14), the energy flowing out of cell $(1,j,k)$ towards the outside of our simulation volume is given by

$$\Delta E^{out,n}_{i,j,k}=\frac{\Delta t}{\Delta r}D_{out}(E^n_{1,j,k}-E^n_{0,j,k}). \tag{16}$$

Here, $E^n_{0,j,k}$ denotes the energy content of a virtual cell belonging to the virtual boundary cell layer at $i=0$. This energy is fed into the virtual cell $(0,j,k)$ as a source term $\Delta E^s_{0,j,k}$, thereby increasing its energy content, and allowed to diffuse and heat up the other virtual cells $(0,j',k')$. By superposition of the contribution originating from all other virtual cells $(0,\mu,\nu)$ during all preceding time steps $\alpha<n$, the energy content of a virtual cell $(0,j,k)$ at time step n is calcuated as

$$\begin{aligned}E^n_{0,j,k} = {} & \sum_{\alpha=0}^{n-1}\sum_{\mu,\nu}\Delta E^{s,\alpha}_{0,\mu,\nu}\cdot\frac{1}{[4\pi D_{out}(n-\alpha)\Delta t]^{3/2}}\\ & \times\exp\left(-\frac{[(\mu-j)^2+(\nu-k)^2]\Delta r^2}{(4\pi D_{out}(n-\alpha)\Delta t)}\right).\end{aligned} \tag{17}$$

These values are then used as the new boundary conditions in order to calculate $\Delta E^{out,n+1}_{1,j,k}$ at the next time step, etc.

The time step Δt used in the numerical integration of Eq. (4) is critical. If Δt is chosen too large, the solution calculated by Eq. (14) becomes unstable. An obvious condition for numerical stability is given by

$$\Delta r^2/\Delta t > D_{max}, \tag{18}$$

where D_{max} denotes the maximum possible value of the diffusivity. With $\Delta r=3$ Å and $D_{max}=180$ cm^2/s, this yields $\Delta t\leqslant 10^{-18}$ s. Attempts using this value, however, were still

hampered by serious stability problems, which were found to disappear only if Δt was reduced to about 10^{-20} s. On the other hand, this time step is unnecessarily small for the MD simulation. Therefore, both computing parts are separated from each other as follows.

First, the particle kinetics are followed up to a total simulated time of 750 fs using our standard molecular dynamics code with dynamical time-step adjustment in the range of $10^{-17}-10^{-15}$ s. In equidistant time steps of $\Delta t^{\mathrm{MD}}=1$ fs, the positions of all particles in the system are stored in a data matrix. After the molecular dynamics trajectory integration has finished, this data matrix is used as input for the explicit finite-differences scheme. In order to accomodate for the much smaller time step, the positions are linearly interpolated within each time interval Δt^{MD}.

The two simulation parts are synchronized by performing in each time interval Δt^{MD} the necessary number of finite-differences time steps. After time intervals of 1 fs the complete set of E as a function of space and time in the solid is output and converted into electronic temperature according to Eq. (8).

In order to limit the memory and CPU time requirements of the code, the boundary conditions are updated in time intervals of 1 fs by means of Eq. (15). Test calculations have shown that a higher boundary refresh rate does not significantly alter the calculated electronic energy density distribution.

III. APPLICATION ON SILVER

Using the formalism described above, the electronic energy density is calculated as a function of time and space for one examplary atomic collision cascade, which is induced by a 5 keV silver atom impinging onto an Ag(111) surface under normal incidence. As already done in our previous study,[13] the impact point was chosen such as to produce a rather rare event associated with high kinetic energy density in the cascade volume, leading to a relatively high sputter yield of 48 atoms. In order to compare the model presented here with the Green's function approach applied earlier,[13] Fig. 2 shows the calculated time dependence of the *surface* electron temperature T_e at a radial distance $r=15$ Å from the impact point for an arbitrarily assumed constant diffusivity $D=20$ cm^2/s. It is seen that the finite differences (FD) calculation predicts a rather sharp initial rise of T_e, which is induced by the highly energetic projectile penetrating the surface layer, thereby locally feeding excitation energy into the electronic system at the impact point. Due to the onset of diffusion, this energy rapidly spreads around the original point of excitation, leading to a pronounced maximum of T_e at times of the order of 10 fs after the impact. Later, the evolution of the collision cascade leads to a spatial spread of kinetic energy and, hence, a stronger delocalization of electronic excitation sources within the crystal volume. In combination with the rapid dissipation of excitation energy, this results in a fast decay of T_e as a function of elapsed time. At $t=750$ fs the electron temperature has decreased to values only slightly above room temperature. At this point, we remark that the fine structure observed in Fig. 2 is not caused by statistical noise, but reflects the kinetics of fast secondary recoil atoms in the uppermost crystal layer.

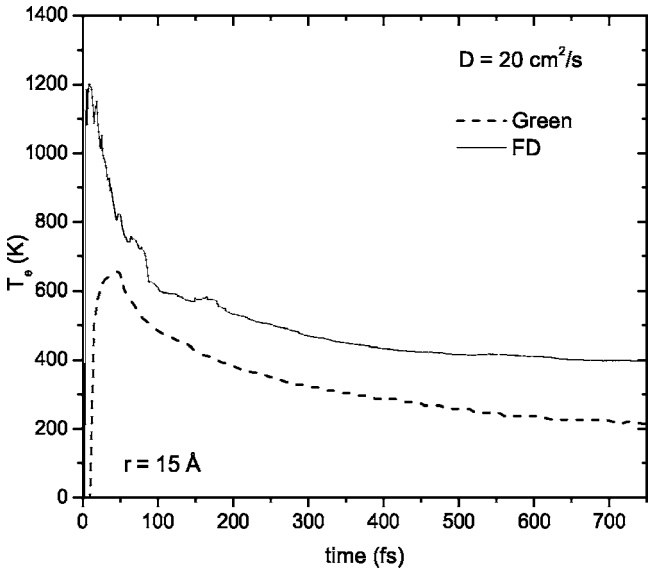

FIG. 2. Time evolution of the surface electron temperature for a radial distance $r=15$ Å from the impact point.

Comparing the FD calculation with the Green's function method, we observe characteristic differences. At small times after the projectile impact, the FD calculation apparently predicts significantly higher electron temperatures. Although not as pronounced, slightly larger temperatures are also predicted at later times. We attribute these observations to the different boundary conditions employed in both types of calculations. More specifically, the Green's function approach generates a full-space solution, whereas the FD calculation correctly incorporates the surface by prohibiting outward energy flow towards the vacuum. As a zero-order approximation, one would therefore expect a factor of 2 between the energy densities calculated with both methods. In combination with Eq. (8), this would translate to $\sqrt{2}$, which is in reasonable agreement with the data presented in Fig. 2.

The FD code now provides a powerful basis to calculate more realistic electron temperatures using a time- and space-resolved diffusivity D. As a prerequisite, Fig. 3 shows the time dependence of the order parameter Λ averaged over two different volumes of the model crystallite. The data depicted by the solid line have been averaged over the total crystallite, whereas the dotted line corresponds to the average taken over a small cubic subvolume of dimension $10\times10\times10$ Å^3 located in the center of the collision cascade (see small sketch depicted in Fig. 3). Here, the crystallographic order is completely destroyed within approximately 350 fs after the particle impact. Apparently, the time scale for this transition is significantly longer in the larger volume, illustrating the highly localized character of the lattice disorder generated in the cascade. This finding illustrates the necessity of a space- and time-resolved determination of Λ in evaluating the local diffusivity via Eq. (13).

Using the same MD data as in Fig. 2, the dynamics of the electron temperature distribution are calculated using the FD code with a space and time resolved diffusivity according to

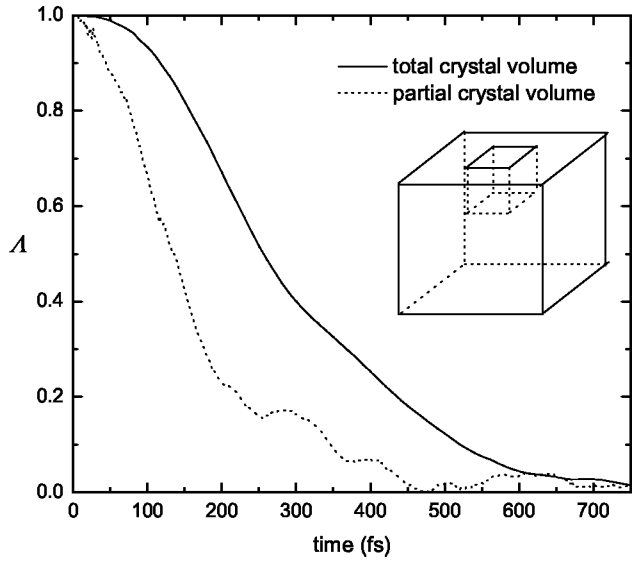

FIG. 3. Local order parameter Λ for two different crystal volumes as a function of time after the projectile impact. The relative size and position of the "partial" crystal volume (dotted line) within the total model crystallite (solid line) is schematically drawn, too.

Eq. (10). As initial conditions, $T_e=0$ K and $T_l=300$ K were chosen. Figure 4 depicts temporal snapshots of the resulting lateral distribution of (a) the electron temperature and (b) the diffusion coefficient D evaluated at the surface; i.e., in the uppermost cell layer of the model crystallite. This particular visualization was chosen, because we are in the long run interested in determining the influence of T_e on excitation or ionization of sputtered particles, which originate predominantly directly from the surface. In order to emphasize the role of lattice dynamics, Fig. 4(c) shows a three-dimensional animation of the corresponding MD trajectory. A more complete set of animations can be viewed electronically at our web address indicated below.

The first set of snapshots is taken at $t=7$ fs, when the projectile still traverses the surface layer, thereby depositing a large amount of excitation energy at the surface. Simultanously, the diffusivity is significantly reduced due to local lattice heating immediately around the impact point. The combination of both effects leads to a relatively high local electron temperature of about 6500 K directly at the impact point.

At 150 fs after the projectile impact, the temporal and spatial evolution of the collision cascade has already led to sputter emission of two surface atoms as well as to significant damage of the crystallographic order within a circular near-surface volume of approximately 10 Å diameter around the original impact point. By inspecting the diffusivity distribution at that time, the correlation between lattice disorder and the magnitude of D becomes clearly visible. More specifically, surface areas of reduced crystallographic order—which in most cases will also be those of an above average lattice temperature—exhibit strongly reduced values of D, whereas the undisturbed regions at the crystal boundaries still reveal diffusion coefficients of 150–180 cm^2/s. The electron temperature at the surface exhibits a much broader distribution in connection with much smaller absolute values, caused mainly by the rapid diffusion of the original excitation. This distribution is superimposed by local excitation sources originating from fast recoil atoms moving within the surface layer.

The next snapshots captured at $t=350$ fs reveal (i) the onset of massive sputtering and (ii) the spatial spread of the collision cascade predominantly propagating in direction towards the front-right crystal edge. Looking at the diffusivity plot, one finds a nearly homogenous distribution with rather low values of $D\approx 0.5-5$ cm^2/s. Only at the upper-right and the back boundary surface edge there are still insular peaks of high diffusivity, in correspondence with the nearly undisturbed crystalline structure in these surface regions. The corresponding electron temperature distribution peaks at values around 1000 K and still shows prominent local structure reflecting the ongoing kinetic heating of the electronic subsystem by fast recoils. Finally, at $t=750$ fs an electron temperature distribution is obtained which exhibits a Gaussian-like shape with a maximum of approximately 2000 K. The location of the maximum excitation correlates with the core of enhanced collision dynamics and crystallographic disorder.

To allow a better visualization of the time dependence of surface excitation, we calculate the temporal evolution of T_e for different radial distances r from the impact point. For more details concerning the averaging procedure, the reader is referred to Ref. 13. The resulting distributions $T_e(t)$ are depicted in Fig. 5 for $r=0,3,6,\ldots,15$ Å.

There are several interesting observations. Shortly after the impact, the predicted excitation exhibits a sharp peak of about 10 fs duration. The maximum electron temperature reached in this time interval is calculated as 6500 K at $r=0$ and decreases with increasing distance from the impact point. After the projectile has passed the surface layer, the electron temperature is found to rapidly decay due to the onset of diffusion without any notable electronic energy source term, until at times of about 50 fs values close to room temperature are reached. Probably the most striking observation in Fig. 5 is the fact that, after this initial decay, the surface excitation is found to rise again, leading to a second maximum of T_e at times around 500 fs.

This finding is of utmost importance, since it reflects the trapping of electronic excitation in a collision cascade by means of local heating and, more important, atomic disorder. The electron temperature reached in the later stage of the cascade is clearly sufficient to influence the ionization and excitation processes of sputtered particles leaving the surface.[28] Moreover, the time scale at which these temperatures are reached coincides almost perfectly with that of maximum particle emission. This fact is demonstrated in Fig. 6, which shows the emission statistics of sputtered particles as a function of time after the projectile impact.

The temporal structure of the electronic excitation determined here can be compared to that calculated by Usman *et al.*,[29] who find a time dependence of T_e that is qualitatively similar to that depicted in Fig. 2. There are, however, distinct

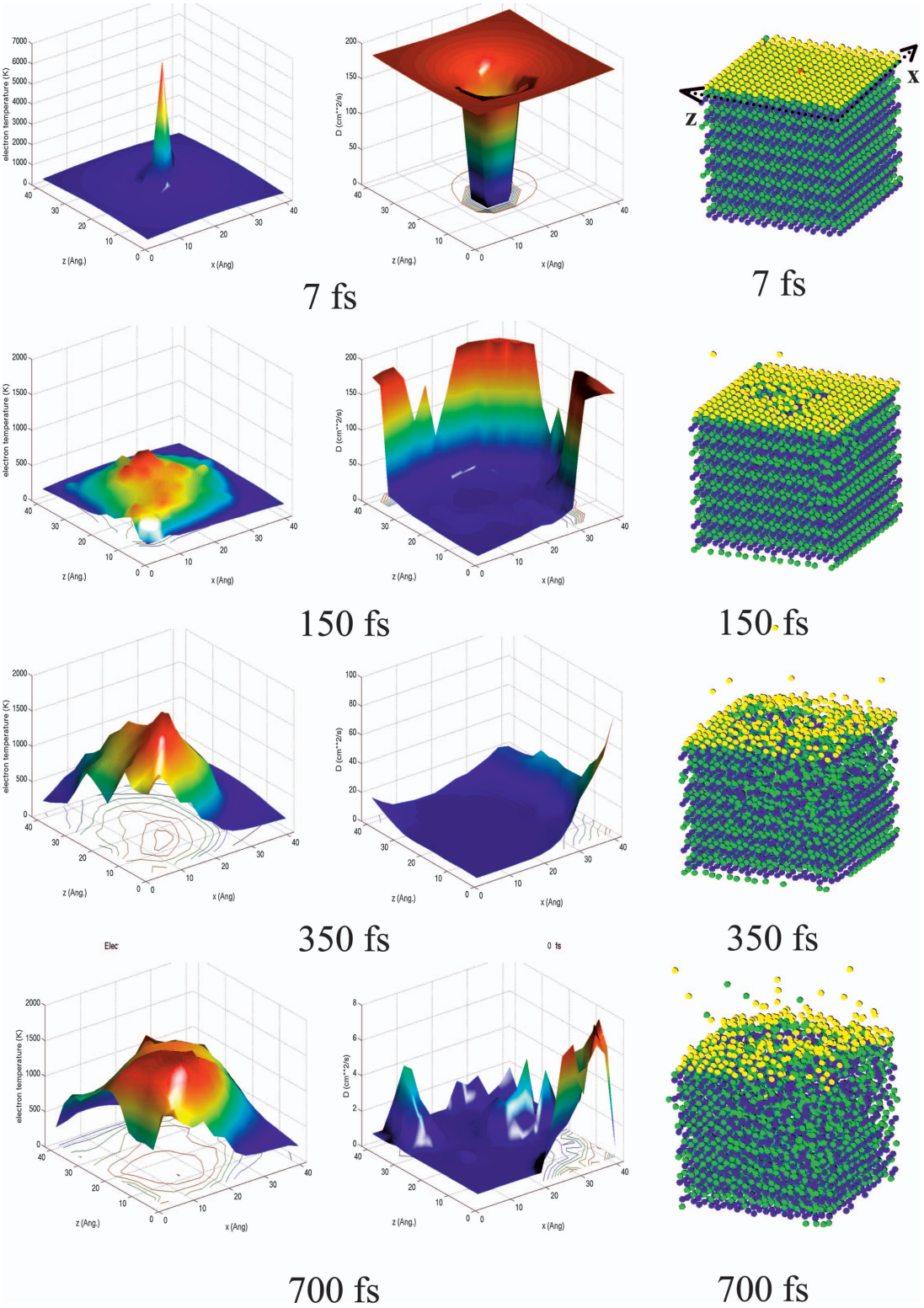

FIG. 4. (Color) Snapshots of (a) the electron temperature T_e and (b) the diffusivity D at the surface. (c) The corresponding trajectory pictures in a perspective view.

differences that will significantly influence the ionization and excitation behavior of sputtered particles. First, the electron temperature calculated in Ref. 29 exhibits its maximum at about 100 fs after the projectile impact; i.e., much later than that depicted in Fig. 2. We attribute this to the rather crude assumptions regarding the particle dynamics of the collision cascade, which form the basis of the kinetic excitation treatment in Ref. 29. Moreover, the effect of local lattice disorder has not been included in Ref. 29, leading to an unrealistically fast decay of T_e at times larger than 200 fs.

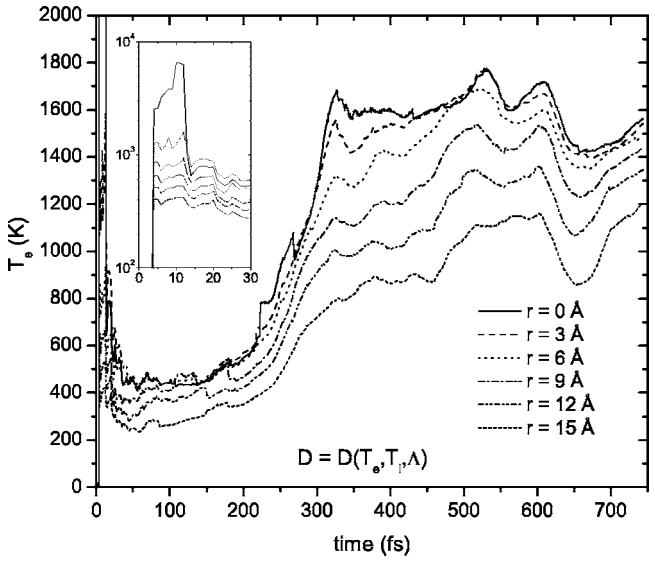

FIG. 5. Time evolution of the surface electron temperature for different radial distances and a diffusion coefficient $D = D(T_e, T_l, \Lambda)$.

IV. CONCLUSION

First results obtained for a selected ion impact event reveal an interesting time structure of the kinetic electronic excitation associated with the particle dynamics in a collision cascade. Immediately following the projectile impact, we find a sharp maximum of about 10 fs width, localized directly at the impact point, where excitation energy densities are reached that translate to electron temperatures of several thousand kelvin. While this maximum appears at times much too short to significantly influence the excitation or ionization states of sputtered particles, it may play a dominating role for projectile induced kinetic electron emission from the surface.

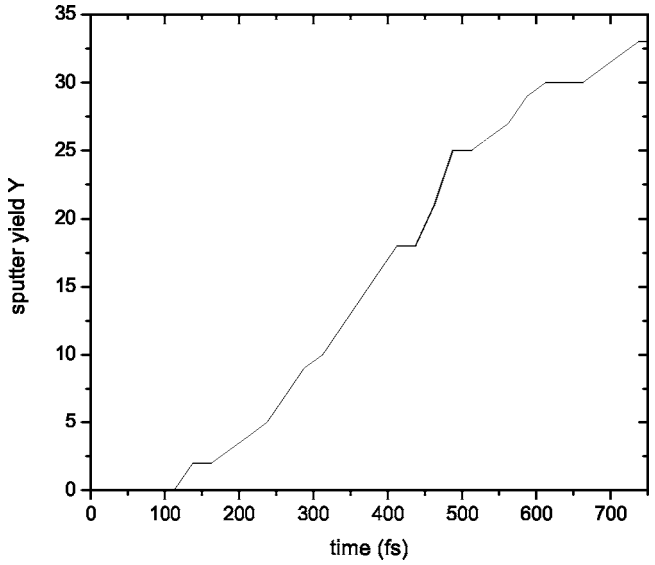

FIG. 6. Sputter yield as a function of time. In order to define the ejection time an atom is considered sputtered as soon as it crosses a plane located at a distance of 7 Å above the surface.

The initial excitation is rapidly dissipated by the onset of fast heat diffusion. If the diffusivity would remain the same as for the undisturbed crystal, this cooling would simply lead to a monotonic decay of the electron temperature on time scales of the order of 100 fs. If, on the other hand, the local and temporal variations of the diffusivity D are taken into account, the excitation energy density is found to rise again, leading to a pronounced second maximum of T_e at times of several hundred femtoseconds after the projectile impact.

We attribute this finding to the influence of local heating and, most important, impact-generated atomic disorder, which are shown to lead to a trapping of the electronic excitation within the crystal volume affected by the collision cascade. From an analysis of the emission statistics of the sputtering process, we conclude that it is this feature that determines the ionization and excitation probabilities of sputtered particles.

Utilizing the combination between MD and the electronic excitation calculation applied here, it is in principle feasible to locate the emission of every single particle leaving the surface both in space and time and to correlate its ionization probability with the electron temperature calculated at this point. This way, characteristics of secondary ion emission can be predicted that are otherwise inaccessible by MD simulations.

We are aware of the fact that there is an additional excitation mechanism by electron promotion in hard collisions between cascade atoms, which has been neglected in the model presented. Since hard collisions can easily be identified in the MD scheme, such effects can in principle be included into our model, for instance, as an additional source term entering Eq. (4). Moreover, the localized core-hole excitations generated that way can in principle be followed in the MD scheme.[4–10,30] Corresponding developments, which will then allow us to estimate the relative role of both excitation mechanisms, are currently under way in our lab.

ACKNOWLEDGMENTS

The authors are greatly indebted to Z. Sroubek for many useful discussions. We would like to thank B.J. Garrison for providing the basis of the molecular dynamics simulation code. We also gladly acknowledge financial and continuous support of this work by the Deutsche Forschungsgemeinschaft within the SFB 616 "Energy dissipation at surfaces." Finally, we thank J. Bloemen, R. Kohn and the RWTH Aachen University Center for Computing and Communication for providing CPU time at the Sun Fire SMP-Cluster.

*Electronic address: wucher@uni-essen.de; URL: http://www.exp.physik.uni-due.de/wucher

[1] W. O. Hofer, Scanning Microsc. Suppl. **4**, 265 (1990).
[2] M. Yu, *Sputtering by Particle Bombardment III*, edited by R. Behrisch and K. Wittmaack (Springer, Berlin, 2001), Chap. 3, pp. 91–154.
[3] M. M. Jakas and D. Harrison, Phys. Rev. B **32**, 2752 (1985).
[4] D. Bernado and B. Garrison, J. Chem. Phys. **97**, 6910 (1992).
[5] D. Bernado, R. Bhatia, and B. Garrison, Comput. Phys. Commun. **80**, 259 (1994).
[6] R. Bhatia and B. J. Garrison, J. Chem. Phys. **100**, 8437 (1994).
[7] I. Wojciechowski and B. J. Garrison, Surf. Sci. **527**, 209 (2003).
[8] M. Shapiro and T. Tombrello, Nucl. Instrum. Methods Phys. Res. B **102**, 277 (1995).
[9] M. Shapiro and T. Tombrello, Nucl. Instrum. Methods Phys. Res. B **90**, 473 (1994).
[10] M. Shapiro and T. Tombrello, Nucl. Instrum. Methods Phys. Res. B **94**, 186 (1994).
[11] H. Urbassek, Nucl. Instrum. Methods Phys. Res. B **122**, 427 (1997).
[12] U. Fano and W. Lichten, Phys. Rev. Lett. **14**, 627 (1965).
[13] A. Duvenbeck, F. Sroubek, Z. Sroubek, and A. Wucher, Nucl. Instrum. Methods Phys. Res. B **225**, 464 (2004).
[14] M. Lindenblatt, E. Pehlke, A. Duvenbeck, Z. Sroubek, and A. Wucher (to be published).
[15] C. Kelchner, D. Halstead, L. Perkins, N. Wallace, and A. DePristo, Surf. Sci. **310**, 425 (1994).
[16] M. Lindenblatt, R. Heinrich, A. Wucher, and B. J. Garrison, J. Chem. Phys. **115**, 8653 (2001).
[17] A. Duvenbeck, M. Lindenblatt, and A. Wucher, Nucl. Instrum. Methods Phys. Res. B **228**, 170 (2005).
[18] J. Lindhard and M. Scharff, Phys. Rev. **124**, 128 (1961).
[19] J. Beck, K. Cole, A. Haji-Sheikh, and B. Litkouhi, *Heat Conduction using Green's Functions*, Series in Computational Methods in Mechanics and Thermal Sciences (Hemisphere, New York, 1992).
[20] X. Y. Wang, D. M. Riffe, Y. S. Lee, and M. C. Downer, Phys. Rev. B **50**, 8016 (1994).
[21] C. Kittel, *Introduction to Solid State Physics* (Wiley & Sons, New York, 1971), p. 249.
[22] V. Veksler, Vacuum **72**, 277 (2004).
[23] L. Verlet, Phys. Rev. **159**, 98 (1967).
[24] P. J. Steinhardt, D. R. Nelson, and M. Ronchetti, Phys. Rev. B **28**, 784 (1983).
[25] T. M. Truskett, S. Torquato, and P. G. Debenedetti, Phys. Rev. E **62**, 993 (2000).
[26] J. Morris and X. Song, J. Phys. C **116**, 9352 (2002).
[27] A. Tveito and R. Winther, *Introduction to Partial Differential Equations: A Computational Approach*, Texts in Applied Mathematics Vol. 29 (Springer-Verlag, Heidelberg, 1998).
[28] Z. Sroubek, Spectrochim. Acta, Part B **44B**, 317 (1989).
[29] E. Y. Usman, Y. T. Matulevich, and I. F. Urazgildin, Vacuum **56**, 293 (2000).
[30] Z. Sroubek, F. Sroubek, A. Wucher, and J. A. Yarmoff, Phys. Rev. B **68**, 115426 (2003).